Nano Energy 128 (2024) 109844

Contents lists available at ScienceDirect

Nano Energy

journal homepage: www.elsevier.com/locate/nanoen

Full paper

Effect of mechanical strain on lateral photovoltaic effect in n-3C-SiC/n-Si hetorjunction Toward mechanical strain sensors capable of photoenergy harvesting

D.H.Dang Tran [a,c,*], Tuan-Hung Nguyen [a], Cong Thanh Nguyen [a], Erik W. Streed [b], Nam-Trung Nguyen [a], Van Thanh Dau [c,**], Dzung Viet Dao [a,c,*]

[a] Queensland Micro, and Nanotechnology Centre, Griffith University, 170 Kessels Road, Brisbane, Queensland 4111, Australia
[b] Institute for Glycomics and Centre for Quantum Dynamics, Griffith University, Parklands Drive, Gold Coast, Queensland 4222, Australia
[c] School of Engineering and Built Environment, Griffith University, Parklands Drive, Gold Coast, Queensland 4222, Australia

ARTICLE INFO

Keywords:
N-type 3C-SiC/n-type Si heterojunction
Photoenergy harvesting
Lateral photovoltaic effect
Strain sensors
Piezo-optoelectronic coupling

ABSTRACT

It is beneficial to have sensors capable of harvesting photoenergy in the era of Internet of Things (IoT) and 5 G integrated infrastructure. In this paper, we report the piezo-optoelectronic coupling characteristic of n-type 3C-SiC/n-type Si heterostructure and demonstrate it with a mechanical strain sensing device capable of harvesting photoenergy. The device is capable of generating a photovoltage as high as 3.4 mV when illuminated by a laser power as small as 10 μW, i.e. four times higher than similar sensors in previous studies. In addition, the strain sensitivity $\Delta V/V/\varepsilon$ ratios are 9.94 and 13.11 for tensile and compressive strain, respectively, which are five times better than conventional metal strain gauges. These findings contribute to the overall understanding of the piezo-optoelectronic coupling effect of SiC/Si heterojunction paving the way for the development of multifunctional sensors with light harvesting capabilities.

1. Introduction

In the era of advanced infrastructure driven by the integration of Internet-of-Things (IoT) and 5 G technologies, it is critical to monitor the surrounding environment through an extensive network of sensors which provide consistent real-time sensing data, allowing us to make proper predictions or decisions that contribute to maintaining a safe, secure and convenient living environment [1]. However, a conventional physical-wired sensor system requires multiple wires to power and transmit sensing data. This approach is costly and labour-consuming to install and maintain, and for some remote area, this becomes a near-impossible challenge. Therefore, there is a high interest in sensors that can harvest energy from surrounding environment and transmit sensing information wirelessly [2,3]. A practical method for sensors to harvest the surrounding photoenergy is by utilizing lateral photovoltaic effect (LPE), which was first discovered by Schottky in 1930 [4] and later developed by Wallmark in 1957 [5]. Since then, the LPE effect has been extensively studied in various semiconductor materials for energy harvesting application [6–14].

Among the materials presenting LPE effect, silicon carbide (SiC) is a wide bandgap material exhibiting many attractive properties such as superior mechanical, chemical, optical and electrical performance [15]. The wide bandgap property not only helps SiC become advantageous in applications requiring high power [16], high working temperature [17], and high frequency [18], but also enables the development of SiC sensors capable of measuring signals in conditions where conventional Si sensors show degradation, such as high-temperature sensor [19], accelerometer [20], or photodetector [12,21–23]. However, the costly fabrication process and small size of 4H-SiC and 6H-SiC present significant challenges, hindering SiC development for applications requiring many sensors [24].

Coupling between multiple physical effects is considered a potential method to enhance the performance of the available sensing techniques. One example is the coupling among piezoelectricity and optoelectronic, known as the piezo-phototronic effect, which enhances the performance of optoelectronic devices by introducing strain modulation in ZnO material [25]. Another method is coupling between piezoresistivity and optoelectronic, known as piezo-optoelectronic effect, has attracted

* Corresponding authors at: School of Engineering and Built Environment, Griffith University, Parklands Drive, Gold Coast, Queensland, 4222, Australia
** Corresponding author.
E-mail addresses: dang.tran@griffithuni.edu.au (D.H.Dang Tran), v.dau@griffith.edu.au (V.T. Dau), d.dao@griffith.edu.au (D.V. Dao).

https://doi.org/10.1016/j.nanoen.2024.109844
Received 22 February 2024; Received in revised form 20 May 2024; Accepted 3 June 2024
Available online 6 June 2024

interest for further enhancing the piezoresistive effect by modulating photogenerated charge carriers in SiC/Si heterojunction [26]. Table S1 in the Supporting Information compares between these coupling methods and traditional mechanical strain sensing techniques.

Recent studies on the piezo-optoelectronic effect focus mainly on p-type SiC/Si heterojunction, as p-type SiC shows better piezoresistive performance than n-type SiC material [27]. However, this leaves a knowledge gap that requires investigation into the mechanical, electrical, and optoelectronic properties of n-type SiC/ n-type Si heterojunction. Additionally, n-type SiC/ n-type Si heterojunctions possess many beneficial properties that should not be overlooked. Firstly, n-type SiC is easier to fabricate using unintentionally doped films method, whereas p-type SiC fabrication requires high temperature (approximately 1350°C), which is nearly the melting temperature of Si [28]. Secondly, in terms of electron-hole pairs separation effect, which is an important effect governing the performance of LPE, the heterostructure of n-type SiC/ n-type Si has more advantages than n-type SiC/ p-type Si heterostructure. Considering n-SiC is the top layer of heterojunction, n-Si substrate is more beneficial for the separation of electrons-holes at the heterojunction than p-Si substrate. Particularly, in the case of n-Si substrate, when laser light is absorbed in Si substrate, more electrons contribute to the generation of LPE, as the generated electrons have a lower recombination probability due to less holes available in the n-Si substrate. In the contrary, for p-Si substrate, the generated electrons easily recombine with the holes available within the p-Si substrate. Therefore, using n-Si substrate produces a better LPE as more electrons are separated at the heterojunction. Because of the above reasons, we decided to investigate and report on the mechanical and electrical properties of n-type SiC/ n-type Si heterojunction.

In this paper, we report the piezo-optoelectronic coupling characteristic of n-type SiC/n-type Si heterostructure and demonstrate it with a mechanical strain sensing device capable of harvesting photoenergy. The ability to collect photoenergy of the device is characterized through lateral photovoltage output measurement, and then the impact of coupling mechanical strain on lateral photovoltaic effect is investigated. The experimental data reveals that the sensing structure exhibits superior light harvesting capabilities, generating a lateral photovoltage as high as 14 mV over 40 μW of laser power, which is three to four times larger than that observed in previous studies, along with excellent mechanical strain sensing capabilities, presenting a $\Delta V/V/\varepsilon$ ratios of 9.94 and 13.11 when applying tensile strain and compressive strain, respectively, which is five times higher than that of conventional metal strain gauges. The underlying mechanism for the piezo-optoelectronic coupling effect is explained based on the photon absorption and carrier diffusion theory. Therefore, the investigation results will significantly contribute to the overall understanding of the properties of SiC material, especially n-type SiC/n-type Si heterojunction, and open up new possibilities for the fabrication of multifunctional sensors with light harvesting capabilities.

The research results and discussions are structured as follows. First, the sensors design concepts, fabrication process, and experimental setup are explained. Then, the photoenergy harvesting capability is characterized. Next, the impact of mechanical strain on the lateral photovoltaic effect is investigated, followed by discussion of the underlying physical explanation. Finally, the highlights of the research are mentioned in the conclusion.

2. The concept of strain sensing using piezo-optoelectronic effect

Fig. 1 illustrates the concept for the light harvesting strain sensor constructed from n-type SiC thin layer grown on n-type Si substrate, forming an n-3C-SiC/n-Si heterostructure, with two aluminium electrodes positioned on the top surface of the SiC thin film. The SiC layer in SiC/Si heterojunction is beneficial for the light harvesting performance, as the SiC layer allows harvesting a wider wavelength spectrum compared to Si/Si homojunction. Additionally, by combining the wide bandgap SiC with narrow bandgap Si, the heterostructure exhibits a large built-in potential which in turn improves the separation of EHPs at the SiC/Si heterojunction [29].

An external laser source of wavelength 637 nm is used to illuminate one end of the sensing element. The SiC layer, with its wide bandgap property, is mostly transparent to the laser wavelength 637 nm, allowing laser light to penetrate into the Si substrate below and be absorbed by the Si substrate [30]. This addition photoenergy leads to the generation of electron-hole pairs (EHPs) within the Si substrate. The generated EHPs are then separated due to the built-in voltage at the SiC/Si heterojunction, resulting in electrons drifting upward to SiC layer and holes drifting downward to Si substrate.

At the illuminated area, the electron concentration within the SiC layer increases (point A), while those at the non-illuminated area remains low (point B). This result in excess electrons diffusing laterally from point A to point B, with lower electron concentration. Two aluminium electrodes positioned at point A and B collect the electrons at these locations. The difference in electrons concentration between the two points results in a lateral photovoltage, V_{AB}, measured between the two electrodes (Fig. 1a).

Applying tensile or compressive strain to the sensing area between the two electrodes alters the electron mobility within the SiC layer, consequently affecting the electron concentration gradient between A and B (Fig. 1b,c). We can estimate the level of strain applied to the sensing area by measuring the changes in the output voltage V_{AB} before and after strain application. This sensing element can be used to constantly monitor the amount of strain applied to the sensor and simultaneously harvest the photoenergy from the external laser source illuminated onto the device.

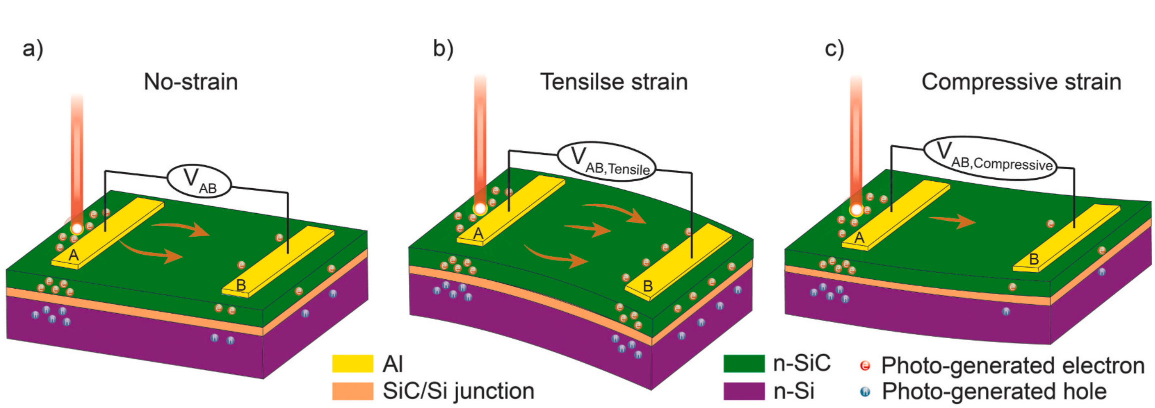

Fig. 1. : Concept of the light-harvesting strain sensor using piezo-optoelectronic effect in case of a) no strain applied, b) under tensile strain and c) under compressive strain.

3. Fabrication and experimental setup

We have fabricated a proof-of-concept device, and the fabrication process comprises eight steps as illustrated in supplementary Figure S1. First, a commercialize n-type Si wafer with a thickness of 380 μm, phosphorous doped with doping concentration of 1×10^{15} atom/cm^3 was used. The Si wafer was thoroughly cleaned following the standard Radio Corporation of America (RCA) cleaning procedure. Then, single-crystalline unintentionally n-type doped 3C-SiC thin films were epitaxially grown on the clean Si wafer using the low-pressure chemical vapor deposition process (LPCVD) at 1000°C, employing propylene (C_3H_6) and silane (SiH_4) as precursors [28]. The thickness of SiC layer was measured using Nanometrics Nanospec 210 instrument, and the value was approximately 500 nm. The doping concentration of SiC layer was measured using hot probe technique [31] and the value was approximately 3×10^{17} atom/cm^3 (Step 2). In the next step, aluminium (Al) was sputtered on top of SiC layer to a thickness of 500 nm, following by a photoresist layer deposited on the top using spin coating method. The electrode designs were subsequently patterned to the photoresist layer by exposing it to ultraviolet light using maskless aligner MLA150 of Heidelberg Instruments. The exposed area became soluble when submerged into developer solution (Step 3–5). We used wet etching method to remove the Al which was not covered by the photoresist mask, forming two Al electrodes on top of the SiC layer with dimensions 200 μm width, 500 μm length, and separated 500 μm from each other (Step 6). The piezoresistive effect in SiC is anisotropic; therefore, to achieve the highest sensitivity, the aluminium electrodes were aligned in <100> orientation, where largest piezoresistive performance is observed for n-type SiC [32]. The excess photoresist was removed using Tegal 915 and the wafer was diced into individual cantilever devices of 40 mm length and 9 mm width (Step 7). Al thin wires were used in the wire bonding process to connect between the electrodes on the device with an external electrical printed circuit board (PCB), improving the ability to handle the device during the characterization experiments (Step 8).

The schematic and geometry of the device are illustrated in supplementary Figure S2a. Supplementary Figure S2b shows a Transmission Electron Microscopy (TEM) image of a cross-section of the device, showing the microstructure at the interface of SiC/Si heterojunction and the thickness of the grown epitaxy 3C-SiC layer was approximately 500 nm. The selected area diffraction (SAED) patterns in supplementary Figure S2c confirm the single crystallinity of the grown 3C-SiC layer.

To characterize the piezo-optoelectronic effect of the heterostructure, we used the bending cantilever method, and the experimental setup is illustrated in Fig. 2. One end of the cantilever was fixed by a c-shape clamp, while the other free-end was hung downward or pull upward using weights, introducing tensile strain or compressive strain to the sensing area, respectively. The weights used were 20 g, 40 g and 60 g, corresponding to the strain values of 154×10^{-6}, 308×10^{-6} and 462×10^{-6}, respectively. The electrical properties were characterized using Keithley 2450 source meter.

The photo-response was tested using laser with wavelength of 637 nm. The laser was mounted on an XYZ stage (PT3, Thorlabs) to fix the laser spot's position inside a u-shape cut out on the clamp. This setup ensured that the laser position remained stable during the strain application experiments. The laser spot diameter was measured using BC100006N-VIS Beam profiler (Thorlabs) and the spot diameter value was 100 μm. Laser power was monitored using S130C power sensors (Thorlabs) and PM100D power meter (Thorlabs). All experiments were conducted under dark conditions and at room temperature (25°C).

4. Result and discussion

First, the current-voltage (I-V) characteristics of the device under dark condition were measured and then the light harvesting ability was evaluated under laser illumination at three powers: 20 μW, 40 μW, and 60 μW (Fig. 3a). The linearity of all four I-V curves indicates that contacts between two aluminium electrodes and the SiC layer are ohmic contacts. Under dark conditions, the I-V curve went through the origin of the coordinates. electrode A of the device with a red laser (wavelength 637 nm), the I-V curve was offset from the origin due to the generation of lateral photovoltage/photocurrent [33].

Fig. 3b shows the generation of the lateral photovoltage (LPV) output under non-uniform illumination of red laser at three powers 20 μW, 40 μW, and 60 μW. In the case of no laser illumination (dark condition), the lateral photovoltage output was 0 mV. Under non-uniform illumination of red laser power 20 μW, the output photovoltage value increased to 7 mV, and kept increasing linearly, reaching 14 mV and 21 mV when increasing the laser power to 40 μW and 60 μW. We could clearly see the excellent repeatability and stable response of the photovoltage output reflecting the laser status when turned on and off. When we shorted the external circuit, we could measure a photocurrent generated across the sensing element, and the short-circuit photocurrent values are shown in Fig. 3c. Under dark conditions, the generated photocurrent was 0 μA, which increased to 2.3 μA under illumination of laser power 20 μW. The negative sign shows that the photogenerated electrons moved within SiC layer from electrode A to B. The generated photocurrent further increased to 4.6 μA and 6.9 μA when increasing the laser power to 40 μW and 60 μW. In Fig. 3d, it can be seen clearly that the output photovoltage scaled linearly with laser power from 0 μW to 500 μW, and eventually reached saturation photovoltage of 97 mV at laser power around 600 μW. Further increasing laser power beyond this point yielded negligible improvement in the photovoltage output. Compared with the previous studies, the lateral photovoltage achieved in this study is approximately three to four times larger than that reported in previous studies [12,33]. The lateral photovoltage performance comparison with other similar devices is summarised in Supplementary Table S2.

The underlying mechanism for the lateral photovoltage output is illustrated in Fig. 4, with Fig. 4a depicting the SiC/Si heterojunction in dark condition, and Fig. 4b-d illustrate the lateral photovoltage forming mechanism when non-uniformly illuminating a red laser beam to the device.

Fig. 4a shows the device consisting of two layers: an n-type SiC layer

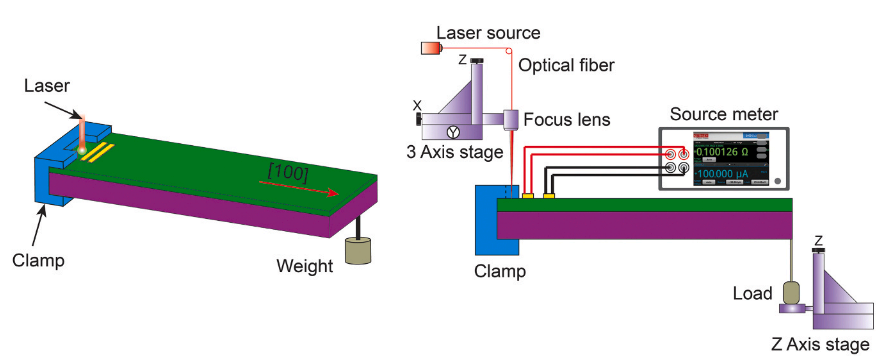

Fig. 2. The experiment setup using bending cantilever method to characterize the piezo-optoelectronic coupling effect of the SiC/Si device.

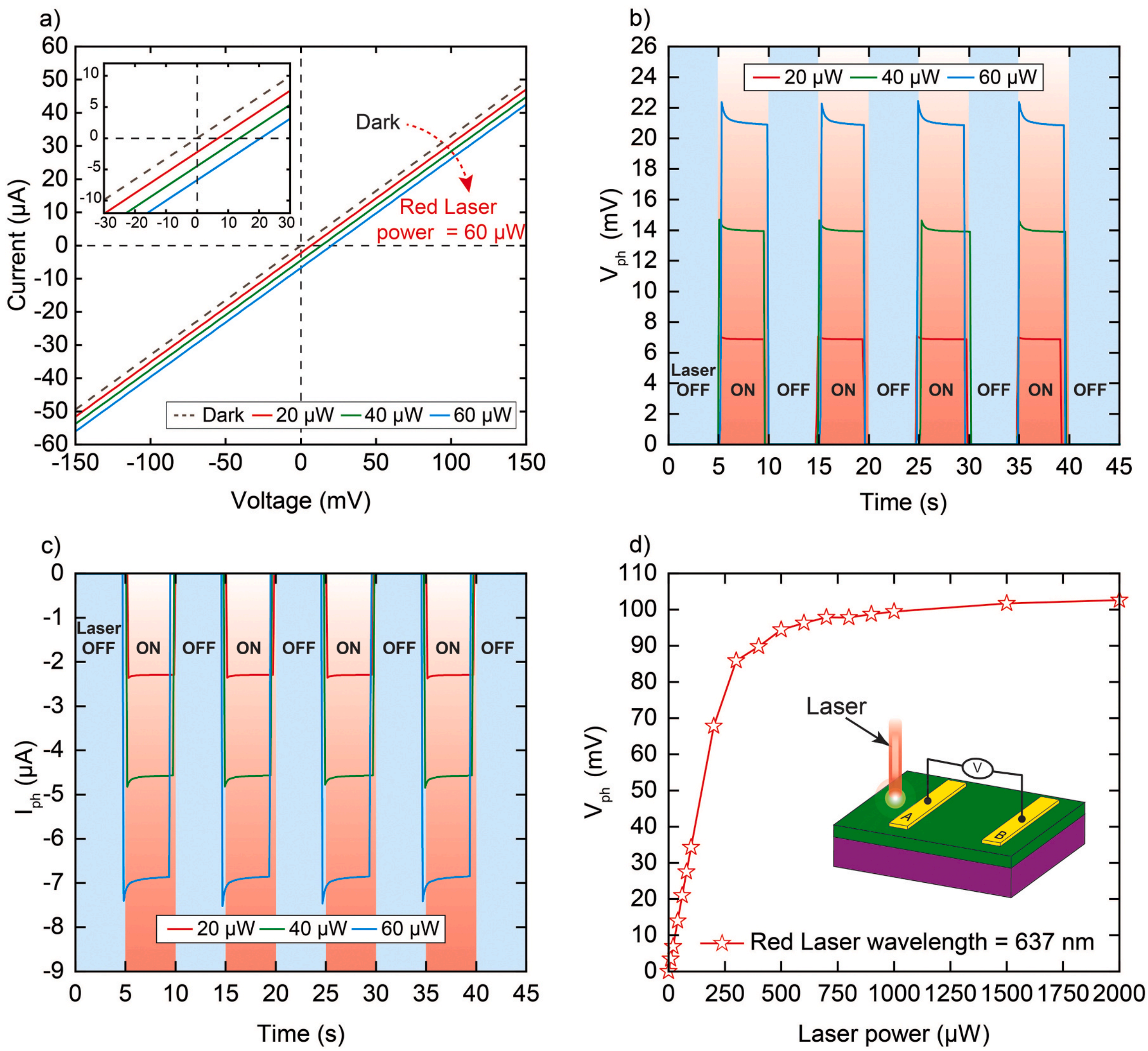

Fig. 3. a) Current-voltage (I-V) characteristic of the device. b) Repeatability test of lateral photovoltage (LPV) generation under illumination of red laser with different power and c) Repeatability test of photocurrent generation under illumination of different laser power. d) Generation of LPV under illumination of laser power increasing from 10 µW to 2000 µW.

deposited on an n-type Si substate. The difference in electron concentration between the Si and SiC layer leads to the movement of electrons and holes across the interface of the two materials [12,34]. Electrons from the SiC layer diffuse through the interface to the Si substrate, leaving positive charges in the SiC layer. Conversely, holes from Si substrate diffuse to the SiC layer, resulting in negative charges in the Si substrate. This migration of electrons and holes eventually reaches equilibrium, creating the depletion zone, at the interface between the two materials. An electric field (E_0) is formed across the depletion zone, preventing further diffusion of electrons and holes through the junction.

Fig. 4b illustrates the underlying mechanism of LPV output generation under non-uniform illumination of red laser wavelength 637 nm to the device. When the red laser light wavelength 637 nm illuminates to the device, it initially contacts with SiC layer. SiC is a wide bandgap material with a bandgap value around 2.38 eV, which is larger than the photoenergy of red laser, value of approximately 1.95 eV. Due to its wide bandgap property, the SiC layer is mostly transparent to the red laser, resulting in the laser passing through the SiC layer and penetrating into the Si substrate below to a depth of approximately 4.2 µm [35] from the SiC/Si interface. The bandgap of Si is 1.12 eV, which is suitable for the absorption of red laser, resulting red laser photons being absorbed by the Si substrate [30]. The laser photons excite the electrons in the Si substrate, allowing them to jump to the conduction band, leaving holes back in the valence band, resulting in generation of electron-hole pairs (EHPs) in Si substrate under the laser spot.

Fig. 4d illustrates the energy band diagrams of the heterojunction at the cross section of electrodes A and B. The built-in electric field across the junction separates the generated electron-hole pairs, causing electrons to drift up toward the SiC layer (opposite to the direction of the built-in electric field), while pushing the holes to drift down towards the Si substrate.

This results in an increase of electron concentration in SiC layer and holes in Si substrate at the laser point, electrode A. However, at non-illuminated area (electrode B), the electron concentration in SiC layer remain unchanged as there are minimal additional EHPs generated. According to the absorption theory [36,37], when illuminate light of frequency ν to a semiconductor with energy gap E_g, the light-excited electrons concentration at the illumination point can be written as:

$$n_0 = K_1(h\nu - E_g)^{\alpha} \quad (1)$$

where K_1 is a proportional coefficient, h is the Planck constant, α is an exponential coefficient. Some of these excited electrons have a chance, R, to recombine with the holes, or re-excited $\tau p/n(0)$ times in average, where τ is the lifetime of diffusion electrons. The electron concentration within SiC layer at laser point is defined as [38]:

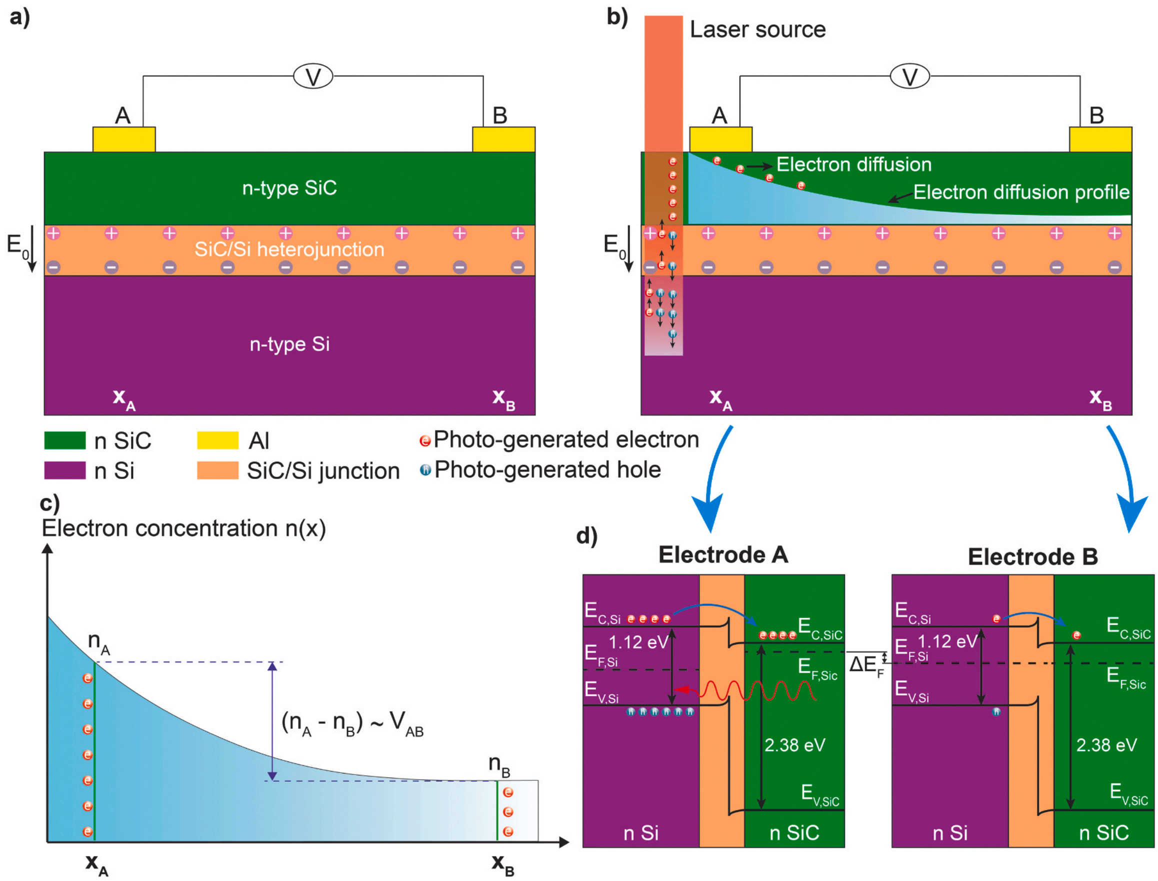

Fig. 4. a) The mechanism of SiC/Si heterojunction form within the device in dark condition and b) The mechanism of lateral photovoltage generation under non-uniform illumination of laser. The LPE includes two phenomena: the generation of electron holes pairs (EHPs) under laser illumination and the electrons diffusion from point A to B within SiC thin layer. c) Diffusion of electrons from A to B due to difference in electron concentration between the two points d) The energy band diagram of SiC and Si layers at laser illuminated region (electrode A), and non-illuminated region (electrode B).

$$N_0 \quad = \quad n_0[1 - R^{(\tau p/n(0))}] \tag{2}$$

Subsequently, the excess electrons in the SiC layer diffuse laterally from the illuminated region (electrode A) to the surrounding circular areas (electrode B) due to the differences in the electron concentration. Along the diffusion path, some electrons interact with holes and recombine, while the remaining electrons are collected at the electrodes A and B. The electrons diffuse laterally within SiC layer to the surrounding area could be described with diffusion model [30,39]:

$$D\frac{d^2N_x}{dx^2} = \frac{N_x}{\tau_{SiC}} \tag{3}$$

where τ_{SiC} is the lifetime of diffusion electrons in SiC. The electron concentration at a certain point distance x on the diffusing path can be defined by:

$$N_x \quad = \quad N_0 \times \exp\left(-\frac{x}{d}\right) \tag{4}$$

where N_0 is the electron concentration at the illumination point, x is the distance from the laser point to the probing position, and $d = (D_{SiC} \times \tau_{SiC})^{1/2}$ is the diffusion length of electron in SiC, with D_{SiC} is the diffusion constant of SiC.

The electron diffusion profile is qualitatively described in Fig. 4c. At the laser illumination point (electrode A), the distance from laser spot to point A is $x_A = 0$, result in the electron concentration at point A is $N_A = N_0$. When x value moves further away from the illumination point (electrode B), the distance from laser spot to point B is $x_B > 0$, the exponential $e^{\left(-\frac{x}{d}\right)}$ value quickly decrease, leading to the exponential decay of the electron concentration. Therefore, the electron concentration at point B becomes significantly smaller compared to point A. shows the difference in electron concentration between point A and B result in the voltage V_{AB} measured across the electrodes, and can be calculated as [39]:

$$\begin{aligned} V_{AB} &= K_2N_0\left[\exp\left(-\frac{|L-x|}{d}\right) - \exp\left(-\frac{|L+x|}{d}\right)\right] \\ &\approx \frac{2K_2N_0}{d} \times \exp\left(-\frac{L}{d}\right)x \end{aligned} \tag{5}$$

where $K_2 = \frac{k_BT}{n_0}$ is the proportional coefficient, x is the laser position, and $2L$ is the distance between the two electrodes.

The mechanical sensing performance of the device was further characterized using weights hanging at the free-end of the cantilever. Force was applied to the free-end of the cantilever using three different weights: 20 g, 40 g and 60 g, resulting in tensile strain (ε) values of 154×10^{-6}, 308×10^{-6} and 462×10^{-6} exerting at the sensing area. Without laser illumination (i.e. in dark condition) these strain values could not be detected, as there was no lateral photovoltage across the sensing area. However, the strain sensing element is activated when non-uniformly illuminating the clamped-end of the cantilever with laser, allowing the lateral photovoltage generation and simultaneously measuring mechanical strain applied to the sensing area.

The strain values applied to the sensor are measured based on the difference between the photovoltage outputs before and after the strain applied. Consider the photovoltage output in the case of free strain as reference, the output photovoltage difference (ΔV) is shown in Fig. 5.

At laser power 20 μW, the output photovoltage in the case of free-strain was 7 mV (Fig. 3b). Introducing tensile strain to the sensing area reduced the photovoltage output by −11 μV, −22 μV, and −32 μV, corresponding to the three weight values 20 g, 40 g and 60 g, respectively (Fig. 5a). Using higher laser power resulted in the photovoltage reducing more significantly (Fig. 5b,c).

Fig. 5d shows an excellent linear relation ($R^2 \approx 99.76\%$) between the output photovoltage and tensile strain (ε) varying from 0 to 500×10^{-6}, with the sensitivity of the mechanical strain sensing element was 0.07 μV/ε, 0.137 μV/ε and 0.207 μV/ε corresponding to laser powers of 20 μW, 40 μW and 60 μW, respectively. It is worth noting that for all three laser power settings 20 μW, 40 μW and 60 μW, we observed a consistent result in fractional changes (ΔV/V) of lateral photovoltage output. The absolute of ΔV/V increased linearly with the applied strain, with the ratios of ΔV/V/ε was 9.94 when tensile strain applied. (Fig. 7a).

Subsequently, a pulley system was used to change the force direction applied to the free end of the cantilever. Three different weights: 20 g, 40 g and 60 g were used to pull up the free end of the cantilever, corresponding to compressive strain (ε) values of 154×10^{-6}, 308×10^{-6} and 462×10^{-6} at the sensing area, respectively. Consider the photovoltage output at free strain as reference, the output photovoltage difference (ΔV) is shown in Fig. 6. Fig. 6a-c clearly show that introducing compressive strain to the sensing area increased the photovoltage output, and the mechanical strain sensitivity also increased when using higher laser power. The sensitivity of the mechanical strain sensing element was 0.088 μV/ε, 0.181 μV/ε and 0.267 μV/ε according with the laser power 20 μW, 40 μW and 60 μW, respectively (Fig. 6d).

Fig. 7 shows the linear relationship between fractional changes of photovoltage output and the tensile strain or compressive strain value varies from 0 to 500×10^{-6} at three different laser powers 20 μW, 40 μW and 60 μW. With all three laser power settings, we can easily see the excellent linear relationship of fractional changes (ΔV/V) of photovoltage output across the range of applied strain. The ratios of ΔV/V/ε was 9.94 for tensile strain and 13.11 for compressive strain, respectively, demonstrating excellent mechanical strain sensing sensitivity which is five times higher than conventional metal strain gauges, which have a typical ratio value only approximately 2 [40].

Based on the theory of energy valleys shifting and electron transfer in SiC conduction band [41], we can qualitatively explain the mechanism for the piezo-optoelectronic coupling effect and illustrated in Fig. 8. Under free-strain condition, the energy valleys have equal energy level and the output voltage measured across electrodes A and B is mainly due to the lateral photovoltage effect (Fig. 8a).

Under a tensile strain along [100] orientation, the energy valleys in direction [100] (i.e., the longitudinal valleys) shifts upward, whereas the energy valleys in direction [010] and [001] (i.e., the transverse valleys) shift downward [41]. These shifts in the six energy valleys result in the repopulation of free electrons from the valleys with high energy to lower energy valleys, meaning that the electrons from the longitudinal direction are redistributed to the valleys in transverse direction. Moreover, since the mobility of electron in transverse direction ($\mu_{\perp}$) is higher than that in the longitudinal direction ($\mu_{\parallel}$) [32], more electrons in the transverse direction ([010] and [001]) lead to a higher total effective mobility, meaning that more electrons move faster towards electrode B. Consequently, the resistance between the two electrodes is reduced, resulting in the reduction of the output voltage V_{AB} (Fig. 8b). Applying higher tensile strain result in more electrons repopulating in the

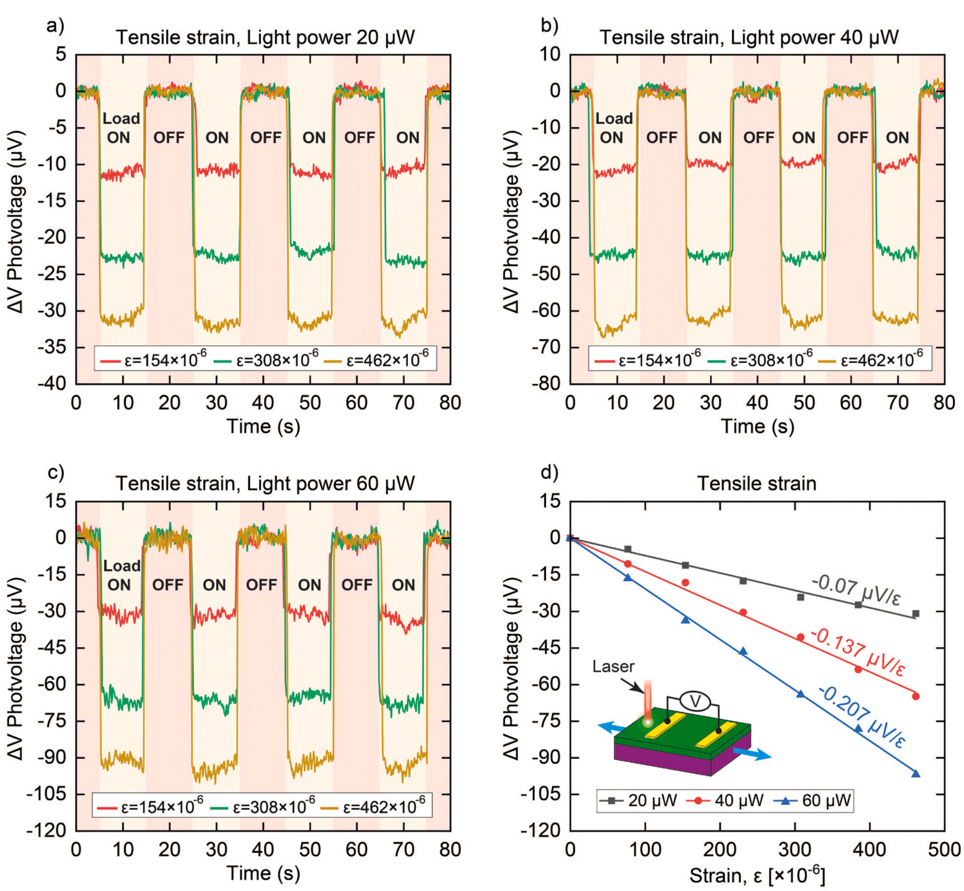

Fig. 5. (a - c) Repeatability test of the photovoltage output under three different tensile strain (ε) value 154×10^{-6}, 308×10^{-6} and 462×10^{-6} with three laser powers 20 μW, 40 μW, and 60 μW. d) The linear change of photovoltage output difference (ΔV) corresponding to tensile strain (ε) varies from 0 to 500×10^{-6} at three different laser power 20 μW, 40 μW and 60 μW.

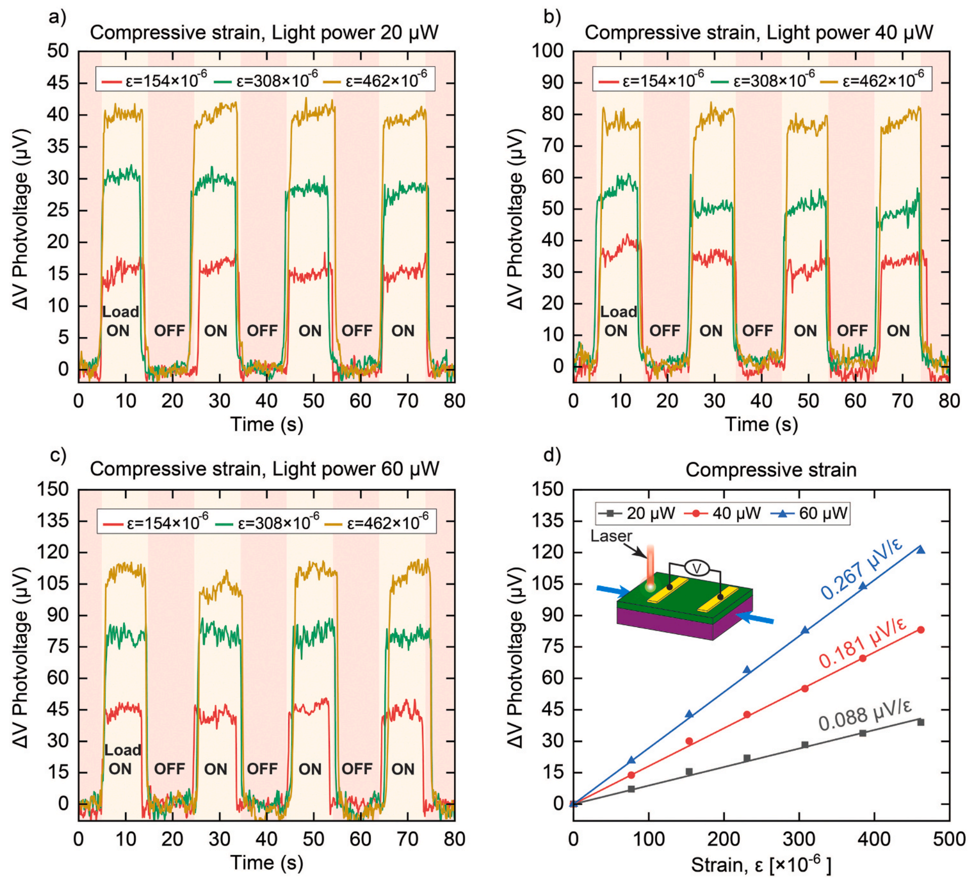

Fig. 6. (a - c) Repeatability test of the photovoltage output under three different compressive strain (ε) value 154×10^{-6}, 308×10^{-6} and 462×10^{-6} with three laser powers 20 μW, 40 μW, and 60 μW. d) The linear change of photovoltage output difference (ΔV) corresponding with compressive strain (ε) varies from 0 to 500×10^{-6} at three different laser power 20 μW, 40 μW and 60 μW.

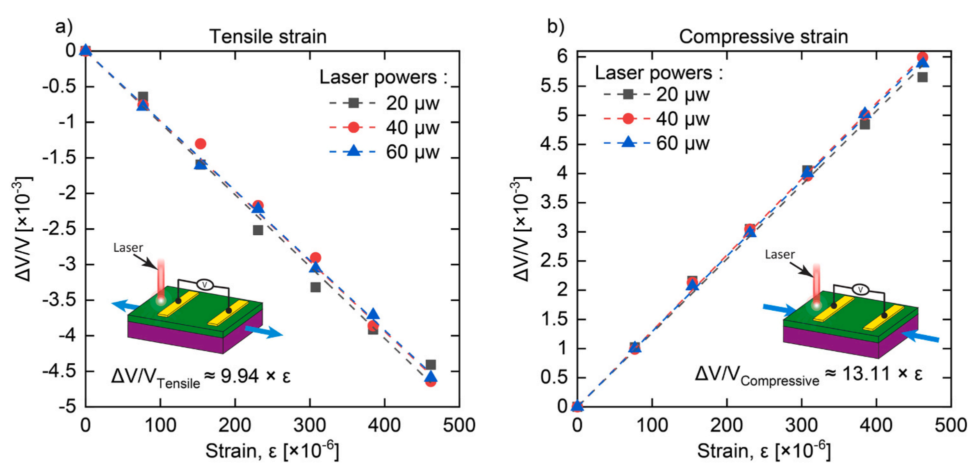

Fig. 7. The linear relationship between fractional changes of lateral photovoltage output and applied strain value in the case of a) tensile strain and b) compressive strain using three laser powers 20 μW, 40 μW and 60 μW.

transverse electron, leading to larger output voltage reduction, and therefore larger ΔV.

On the contrary, under compressive strain, the energy valleys in direction [100] shift downward, while the energy valleys in direction [010] and [001] shift upward. These shifts result in the repopulation of free electrons from the valleys in transverse direction to the valleys in the longitudinal direction, leading to lower total effective mobility, meaning fewer electrons arrive at electrode B. Consequently, the resistance between the two electrodes is increased, resulting in an increase of the output voltage V_{AB} (Fig. 8c). This hypothesis agrees well with the experimental results where V_{AB} decreased (ΔV became negative) when tensile strain was applied, and V_{AB} increased (ΔV became positive) when compressive strain was applied to the cantilever device.

5. Conclusion

In conclusion, we have investigated the impact of mechanical strain on lateral photovoltaic effect in n-type SiC/n-type Si heterojunction and

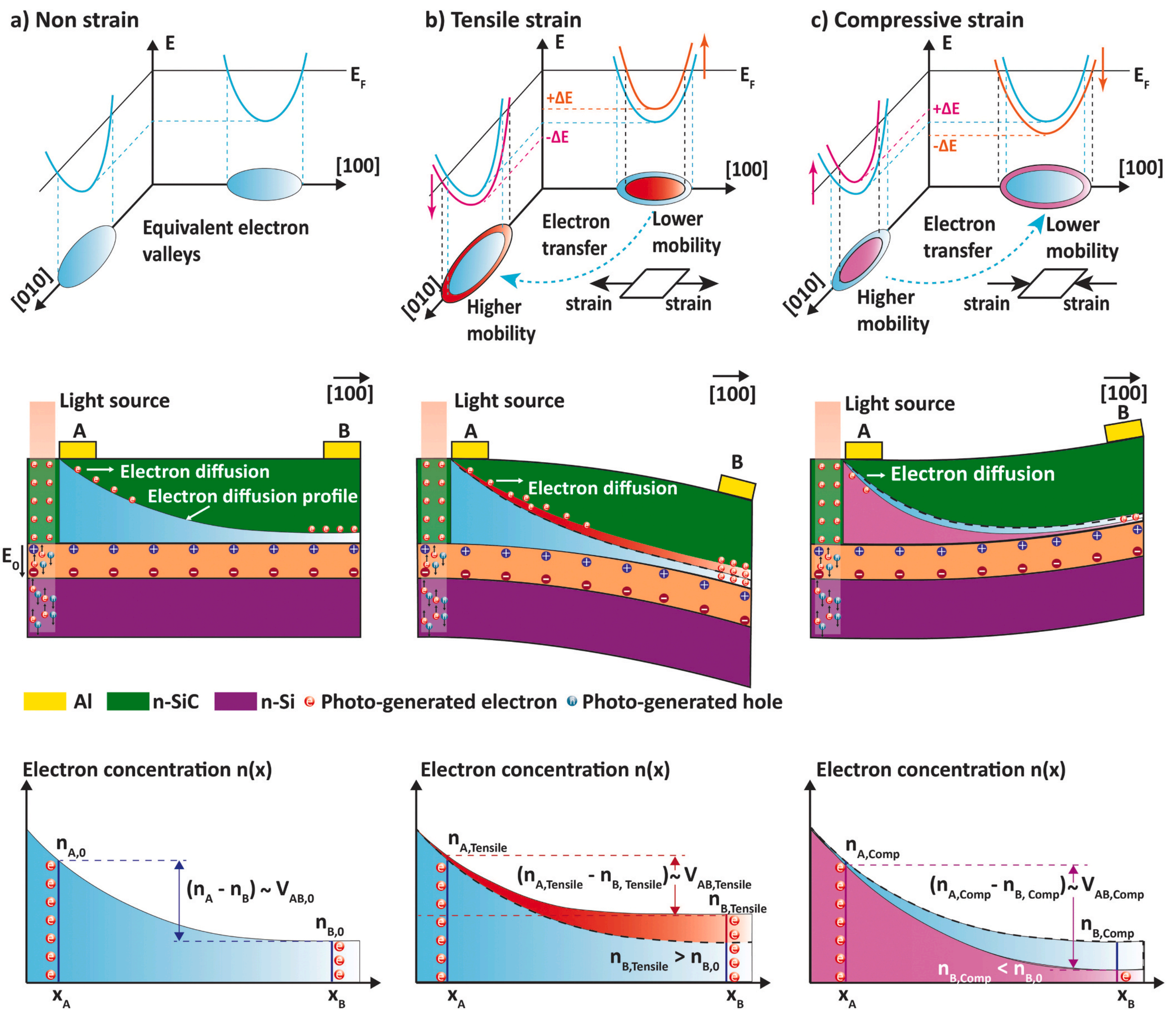

Fig. 8. The mechanism of the piezo-optoelectronic coupling effect under a) non-strain, b) tensile strain and c) compressive strain conditions.

its application for mechanical strain sensors with photoenergy harvesting capabilities. A proof-of-concept cantilever device has been successfully designed and fabricated, featuring a simple yet robust design which consistently sensed the external strain applied while simultaneously harvested the photoenergy exposed to the sensing element. The sensing structure demonstrated superior light harvesting capabilities, generating three to four times larger lateral photovoltage output than that observed in previous studies. Under non-uniform illumination of red laser wavelength 637 nm with power as low as 10 μW, the sensing structure was capable of outputting a lateral photovoltage up to 3.4 mV, which kept increasing linearly, reaching 7 mV, 14 mV, and 21 mV when increasing the laser power to 20 μW, 40 μW and 60 μW, respectively. The device also demonstrated excellent mechanical strain sensing capabilities, with a strain sensitivity $\Delta V/V/\varepsilon$ ratios was 9.94 for tensile strain and 13.11 for compressive strain. This is five times more sensitive than that of conventional metal strain gauges.

The proposed device exhibits excellent repeatability in light harvesting and strain sensing performance. It also shows great long-term performance stability, as consistent results were observed during the experiments period, and repeatable results were achieved months later. The mechanism for light harvesting and strain sensing capabilities have been explained based on absorption theory and diffusion theory, which consistently aligned with our experimental results.

Investigating a full theoretical analysis model to quantitatively explain the effect of strain on the energy band structure of SiC under photo excitation is essential for developing future mechanical strain sensors and will be our future works. The findings in this study remarkably contribute to the overall understanding of the piezo-optoelectronic coupling effect of SiC/Si heterojunction, paving the way toward the development of multifunctional sensors with light harvesting capabilities.

CRediT authorship contribution statement

Dang D.H. Tran: Writing – review & editing, Writing – original draft, Visualization, Validation, Methodology, Investigation, Formal analysis, Data curation, Conceptualization. **Tuan-Hung Nguyen:** Writing – review & editing, Resources, Investigation, Formal analysis, Conceptualization. **Dzung Viet Dao:** Writing – review & editing, Validation, Supervision, Resources, Project administration, Funding acquisition. **Cong Thanh Nguyen:** Writing – review & editing, Validation, Resources, Formal analysis. **Erik W. Streed:** Resources, Project administration, Funding acquisition. **Nam-Trung Nguyen:** Project administration, Funding acquisition. **Van Thanh Dau:** Writing – review & editing, Supervision, Resources, Funding acquisition.

Declaration of Competing Interest

The authors declare that they have no known competing financial interests or personal relationships that could have appeared to influence the work reported in this paper.

Data Availability

Data will be made available on request.

Acknowledgements

This work was supported by the Australian Research Council under Discovery Projects (DP220101252). This work used the Queensland node of the NCRIS-enabled Australian National Fabrication Facility (ANFF). The 3C-SiC/Si material was developed and supplied by the Queensland Micro and Nanotechnology Centre, part of the Queensland node-Griffith-of the Australian National Fabrication Facility, a company established under the National Collaborative Research Infrastructure Strategy to provide nano and microfabrication facilities for Australia's researchers. The sensing devices were also fabricated at the Queensland Micro and Nanotechnology Centre with the support of Nhat-Khuong Nguyen and Pradip Singha. The TEM and SAED images were implemented by Centre for Microscopy and Microanalysis, The University of Queensland, Australia. The experiments were conducted with the support of lab members: Trung-Hieu Vu, Hoai-Duc Vu, Dinh Gia Ninh and Braiden Tong. The authors are grateful for all supports of research centres and research funds.

Appendix A. Supporting information

Supplementary data associated with this article can be found in the online version at doi:10.1016/j.nanoen.2024.109844.

References

[1] Y. Tang, Y. Zhao, H. Liu, Room-temperature semiconductor gas sensors: challenges and opportunities, /12/23 2022, ACS Sens. vol. 7 (12) (2022) 3582–3597, https://doi.org/10.1021/acssensors.2c01142.
[2] T.-H. Nguyen, et al., Giant Lateral photovoltage in a SiC/Si heterojunction with a micro free-standing sic serpentine beam, /08/22 2022, ACS Appl. Energy Mater. vol. 5 (8) (2022) 9830–9836, https://doi.org/10.1021/acsaem.2c01552.
[3] S. Bairagi, I. Shahid ul, M. Shahadat, D.M. Mulvihill, W. Ali, Mechanical energy harvesting and self-powered electronic applications of textile-based piezoelectric nanogenerators: a systematic review, /06/15/ 2023, Nano Energy vol. 111 (2023) 108414, https://doi.org/10.1016/j.nanoen.2023.108414.
[4] W. Schottky, Über den entstehungsort der photoelektronen in kupfer-kupfer-oxydul-photozellen, Phys. Z. vol. 31 (1930) 913.
[5] J.T. Wallmark, A new semiconductor photocell using lateral photoeffect, Proc. IRE vol. 45 (4) (1957) 474–483, https://doi.org/10.1109/JRPROC.1957.278435.
[6] R.H. Willens, Photoelectronic and electronic properties of Ti/Si amorphous superlattices, Appl. Phys. Lett. vol. 49 (11) (1986) 663–665, https://doi.org/10.1063/1.97561.
[7] B.F. Levine, R.H. Willens, C.G. Bethea, D. Brasen, Lateral photoeffect in thin amorphous superlattice films of Si and Ti grown on a Si substrate, Appl. Phys. Lett. vol. 49 (22) (1986) 1537–1539, https://doi.org/10.1063/1.97274.
[8] M. Ogita, K. Kawamura, T. Yamada, T. Yamamoto, Some aspects of position-sensitive photodetectors made of amorphous silicon, Electron. Commun. Jpn. (Part II: Electron.) vol. 70 (5) (1987) 107–114, https://doi.org/10.1002/ecjb.4420700512.
[9] N. Tabatabaie, M.H. Meynadier, R.E. Nahory, J.P. Harbison, L.T. Florez, Large lateral photovoltaic effect in modulation-doped AlGaAs/GaAs heterostructures, Appl. Phys. Lett. vol. 55 (8) (1989) 792–794, https://doi.org/10.1063/1.101762.
[10] J. Lu, H. Wang, Large lateral photovoltaic effect observed in nano Al-doped ZnO films, /07/18 2011, Opt. Express vol. 19 (15) (2011) 13806–13811, https://doi.org/10.1364/OE.19.013806.
[11] A.R.M. Foisal, et al., Ultra-sensitive self-powered position-sensitive detector based on horizontally-aligned double 3C-SiC/Si heterostructures, /01/01/ 2021, Nano Energy vol. 79 (2021) 105494, https://doi.org/10.1016/j.nanoen.2020.105494.
[12] T.-H. Nguyen, et al., Effect of 3C-SiC layer thickness on lateral photovoltaic effect in 3C-SiC/Si heterojunction, IEEE Sens. J. vol. 23 (3) (2023) 2063–2069, https://doi.org/10.1109/jsen.2022.3232318.
[13] T.H. Nguyen, et al., Generation of a charge carrier gradient in a 3C-SiC/Si heterojunction with asymmetric configuration, /11// 2021, ACS Appl. Mater. Interfaces vol. 13 (46) (2021) 55329–55338, https://doi.org/10.1021/acsami.1c15942.
[14] T.-H. Nguyen, et al., Enhanced lateral photovoltaic effect in 3C-SiC/Si heterojunction under external electric field, /12/01/ 2023, Sens. Actuators A: Phys. vol. 363 (2023) 114746, https://doi.org/10.1016/j.sna.2023.114746.
[15] Y. Qie, S. Wang, Q. Sun, Three dimensional metallic porous SiC4 allotropes: stability and battery applications, /09/01/ 2019, Nano Energy vol. 63 (2019) 103862, https://doi.org/10.1016/j.nanoen.2019.103862.
[16] Q. Wu, Y. Zhao, T. Xun, H. Yang, W. Huang, Initial test of optoelectronic high power microwave generation from 6H-SiC photoconductive switch, IEEE Electron Device Lett. vol. 40 (7) (2019) 1167–1170, https://doi.org/10.1109/LED.2019.2918954.
[17] H.-P. Phan, et al., High temperature silicon-carbide-based flexible electronics for monitoring hazardous environments, /07/15/ 2020, J. Hazard. Mater. vol. 394 (2020) 122486, https://doi.org/10.1016/j.jhazmat.2020.122486.
[18] V. Parshin, et al., Silicon carbide for high-power applications at MM and THz ranges, /11/01/ 2017, Diam. Relat. Mater. vol. 80 (2017) 1–4, https://doi.org/10.1016/j.diamond.2017.09.007.
[19] T. Dinh, et al., Unintentionally doped epitaxial 3C-SiC(111) nanothin film as material for highly sensitive thermal sensors at high temperatures, /4// 2018, IEEE Electron Device Lett. vol. 39 (4) (2018) 580–583, https://doi.org/10.1109/LED.2018.2808329.
[20] T. Nguyen, et al., Self-powered monolithic accelerometer using a photonic gate, /10// 2020, Nano Energy vol. 76 (2020), https://doi.org/10.1016/j.nanoen.2020.104950.
[21] H. Bencherif, L. Dehimi, G. Messina, P. Vincent, F. Pezzimenti, F.G.D. Corte, An optimized Graphene/4H-SiC/Graphene MSM UV-photodetector operating in a wide range of temperature, /06/01/ 2020, Sens. Actuators A: Phys. vol. 307 (2020) 112007, https://doi.org/10.1016/j.sna.2020.112007.
[22] M.L. Megherbi, et al., An efficient 4H-SiC photodiode for UV sensing applications, Electronics vol. 10 (20) (2021) 2517 [Online]. Available: https://www.mdpi.com/2079-9292/10/20/2517.
[23] H. Bencherif, et al., Improving graphene/4H-SiC/graphene MSM UV photodetector sensitivity using interdigitated electrodes formalism and embedded gold plasmonic nanoparticles, /04/01/ 2022, Opt. Laser Technol. vol. 148 (2022) 107683, https://doi.org/10.1016/j.optlastec.2021.107683.
[24] P. Tanner, et al., Excellent rectifying properties of the n-3C-SiC/p-Si heterojunction subjected to high temperature annealing for electronics, MEMS, and LED applications, /12// 2017, Sci. Rep. vol. 7 (1) (2017), https://doi.org/10.1038/s41598-017-17985-9.
[25] W. Wu, Z.L. Wang, Piezotronics and piezo-phototronics for adaptive electronics and optoelectronics, /05/10 2016, Nat. Rev. Mater. vol. 1 (7) (2016) 16031, https://doi.org/10.1038/natrevmats.2016.31.
[26] A.R. Md Foisal, et al., Pushing the limits of piezoresistive effect by optomechanical coupling in 3C-SiC/Si heterostructure, /11// 2017, ACS Appl. Mater. Interfaces vol. 9 (46) (2017) 39921–39925, https://doi.org/10.1021/acsami.7b12128.
[27] H.P. Phan, D.V. Dao, K. Nakamura, S. Dimitrijev, N.T. Nguyen, The piezoresistive effect of SiC for MEMS sensors at high temperatures: a review, /12// 2015, J. Micro Syst. vol. 24 (2015) 1663–1677, https://doi.org/10.1109/JMEMS.2015.2470132.
[28] L. Wang, S. Dimitrijev, J. Han, P. Tanner, A. Iacopi, L. Hold, Demonstration of p-type 3C–SiC grown on 150mm Si(100) substrates by atomic-layer epitaxy at 1000°C, /08/15/ 2011, J. Cryst. Growth vol. 329 (1) (2011) 67–70, https://doi.org/10.1016/j.jcrysgro.2011.06.041.
[29] H. Nguyen, et al., Effects of photogenerated-hole diffusion on 3C-SiC/Si heterostructure optoelectronic position-sensitive detector, /7// 2021, J. Phys. D: Appl. Phys. vol. 54 (26) (2021), https://doi.org/10.1088/1361-6463/abf3ff.
[30] A.R.M. Foisal, et al., 3C-SiC/Si heterostructure: an excellent platform for position-sensitive detectors based on photovoltaic effect, /10/30 2019, ACS Appl. Mater. Interfaces vol. 11 (43) (2019) 40980–40987, https://doi.org/10.1021/acsami.9b15855.
[31] P. Tanner, et al., Novel electrical characterization of thin 3C-SiC films on Si substrates, 07/01, Sci. Adv. Mater. vol. 6 (2014), https://doi.org/10.1166/sam.2014.1813.
[32] J.S. Shor, D. Goldstein, A.D. Kurtz, Characterization of n-type beta -SiC as a piezoresistor, IEEE Trans. Electron Devices vol. 40 (6) (1993) 1093–1099, https://doi.org/10.1109/16.214734.
[33] T. Nguyen, et al., The concept of light-harvesting, self-powered mechanical sensors using a monolithic structure, /6// 2022, Nano Energy vol. 96 (2022), https://doi.org/10.1016/j.nanoen.2022.107030.
[34] A.R. Md Foisal, et al., Photoresponse of a highly-rectifying 3C-SiC/Si heterostructure Under UV and visible illuminations, /8// 2018, IEEE Electron Device Lett. vol. 39 (8) (2018) 1219–1222, https://doi.org/10.1109/LED.2018.2850757.
[35] M.A. Green, M.J. Keevers, Optical properties of intrinsic silicon at 300 K, Prog. Photovolt.: Res. Appl. vol. 3 (3) (1995) 189–192, https://doi.org/10.1002/pip.4670030303.
[36] T.-H. Nguyen, et al., Ultrasensitive self-powered position-sensitive detector based on n-3C-SiC/p-Si heterojunctions, /02/22 2022, ACS Appl. Electron. Mater. vol. 4 (2) (2022) 768–775, https://doi.org/10.1021/acsaelm.1c01156.
[37] J.I. Pankove, Optical processes in semiconductors, Courier Corporation, 1975.

[38] C.Q. Yu, H. Wang, Large near-infrared lateral photovoltaic effect observed in Co/Si metal-semiconductor structures, Appl. Phys. Lett. vol. 96 (17) (2010), https://doi.org/10.1063/1.3419903.
[39] C.Q. Yu, H. Wang, S.Q. Xiao, Y.X. Xia, Direct observation of lateral photovoltaic effect in nano-metal-films, /11/23 2009, Opt. Express vol. 17 (24) (2009) 21712–21722, https://doi.org/10.1364/OE.17.021712.
[40] A.C.H. Rowe, Piezoresistance in silicon and its nanostructures, J. Mater. Res. vol. 29 (6) (2014) 731–744, https://doi.org/10.1557/jmr.2014.52.
[41] H.-P. Phan, et al., Strain effect in highly-doped n-Type 3C-SiC-on-glass substrate for mechanical sensors and mobility enhancement, Phys. Status Solidi (a) vol. 215 (24) (2018) 1800288, https://doi.org/10.1002/pssa.201800288.

D.H. Dang Tran received his B.E. in Automation Technology from HCMC University of Technology and Education, Vietnam, in 2014, and M.Sc. degree in Mechatronic and Sensors Systems Technology from Karlsruhe University of Applied Sciences, Germany, in 2018. From 2018 to 2022, he worked for a top semiconductor company in Japan as sensor products specialist before pursuing his Ph.D. degree at Queensland Micro- and Nanotechnology Centre, Griffith University, QLD, Australia, from 2022, researching on silicon carbide (SiC) material for sensor applications. His main research interest includes MEMS Sensors, silicon carbide MEMS/NEMS, and sensors systems.

Tuan-Hung Nguyen is currently a Postdoctoral Research Fellow at Queensland Micro- and Nanotechnology Centre, Griffith University, Australia, where he received his Ph.D. He received his M.S and B.E degrees in mechanical engineering from Seoul National University of Science and Technology, Korea and Hanoi University of Science and Technology, Vietnam, respectively. His research interests are optoelectronic MEMS sensors, silicon carbide MEMS/NEMS, and optomechatronic systems. He was awarded the competitive Griffith University Postgraduate Research Scholarship (GUPRS) and Griffith University International Postgraduate Research Scholarship (GUIPRS). His works were featured several times on the covers of prestigious journals.

Cong Thanh Nguyen is currently a Research Fellow in the School of Engineering and Built Environment, Griffith University, Australia. He received his PhD in Mechanical and Mechatronic Engineering from University of Technology Sydney, in 2021. His research interests include micro-electro-mechanical systems (MEMS), silicon carbide MEMS for harsh environments, physics of semiconductors, self-powered and energy-harvesting sensors, and composite materials and structures.

Erik W. Streed is a physicist in Griffith University's School of Environment and Science, the Deputy Director of the Centre for Quantum Dynamics, and a Research Leader in the Institute for Glycomics. He is best known for his pioneering work in integrating diffractive optics with trapped ions, which lead to the first imaging of a single atom's shadow. A graduate of Caltech (BSc Physics) and MIT (PhD Physics), he completed his graduate work in Bose-Einstein condensate in the group of Wolfgang Ketterle (Physics Nobel 2001).

Nam-Trung Nguyen is an Australian Laureate Fellow. He received his Dipl-Ing, Dr Ing, and Dr Ing Habil degrees from Chemnitz University of Technology, Germany, in 1993, 1997, and 2004, respectively. From 1999 to 2013, he was an Associate Professor at Nanyang Technological University in Singapore. Since 2013, he has served as a Professor and the Director of Queensland Micro- and Nanotechnology Centre of Griffith University, Australia. He is a Fellow of ASME and a Senior Member of IEEE. His research is focused on microfluidics, nanofluidics, micro/nanomachining technologies, micro/nanoscale science, and instrumentation for biomedical applications.

Van Thanh Dau received his B.S. degree in aerospace engineering from Hochiminh City University of Technology, Vietnam, in 2002, and Ph.D. degree in MEMS from Ritsumeikan University, Japan, in 2007. He was a Postdoctoral Fellow with Japan Society for the Promotion of Science and then a Research Scientist at Sumitomo Chemical until 2018. He is currently with School of Engineering and Built Environment, Griffith University, Australia. Van is the author and coauthor of more than 200 scientific articles and 25 inventions (9 US patents). His research interests include MEMS and electrohydrodynamics.

Dzung Viet Dao received his PhD degree in Micro Electro Mechanical Systems (MEMS) from Ritsumeikan University, Japan in 2003. He served as a Postdoctoral Research Fellow from 2003 to 2006, Lecturer from 2006 to 2007, and Chair Professor from 2007 to 2011, all at Ritsumeikan University, Japan. From 2011 Dr Dao joined Griffith University, Australia, as a Professor in the School of Engineering and Built Environment, where he is currently teaching Mechatronics and Mechanical Engineering. His current research interests include advanced sensing effects in nano materials, MEMS sensors & actuators, sensors for harsh environment, and wireless sensor network..